

# ENVIRONMENTAL RESEARCH LETTERS

---

LETTER • OPEN ACCESS

## Association between NO<sub>2</sub> concentrations and spatial configuration: a study of the impacts of COVID-19 lockdowns in 54 US cities

To cite this article: Man Sing Wong *et al* 2021 *Environ. Res. Lett.* **16** 054064

View the [article online](#) for updates and enhancements.

**ENVIRONMENTAL RESEARCH LETTERS****OPEN ACCESS****RECEIVED**  
6 December 2020**REVISED**  
23 March 2021**ACCEPTED FOR PUBLICATION**  
30 March 2021**PUBLISHED**  
11 May 2021

Original Content from  
this work may be used  
under the terms of the  
[Creative Commons  
Attribution 4.0 licence](#).

Any further distribution  
of this work must  
maintain attribution to  
the author(s) and the title  
of the work, journal  
citation and DOI.

**LETTER**

# Association between NO<sub>2</sub> concentrations and spatial configuration: a study of the impacts of COVID-19 lockdowns in 54 US cities

Man Sing Wong<sup>1,2</sup>, Rui Zhu<sup>1,3,\*</sup> , Coco Yin Tung Kwok<sup>1</sup> , Mei-Po Kwan<sup>4</sup>, Paolo Santi<sup>5,6</sup>, Chun Ho Liu<sup>7</sup>, Kai Qin<sup>8</sup>, Kwon Ho Lee<sup>9</sup> , Joon Heo<sup>10</sup>, Hon Li<sup>1</sup> and Carlo Ratti<sup>5</sup>

<sup>1</sup> Department of Land Surveying and Geo-Informatics, The Hong Kong Polytechnic University, Kowloon, Hong Kong Special Administrative Region of China, People's Republic of China

<sup>2</sup> Research Institute for Sustainable Urban Development, The Hong Kong Polytechnic University, Kowloon, Hong Kong Special Administrative Region of China, People's Republic of China

<sup>3</sup> Senseable City Laboratory, Future Urban Mobility, Singapore-MIT Alliance for Research and Technology, 1 Create Way, 09-02 Create Tower, 138062, Singapore

<sup>4</sup> Institute of Space and Earth Information Science, The Chinese University of Hong Kong, Hong Kong Special Administrative Region of China, People's Republic of China

<sup>5</sup> Senseable City Laboratory, Department of Urban Studies and Planning, Massachusetts Institute of Technology, Cambridge, MA 02139, United States of America

<sup>6</sup> Istituto di Informatica e Telematica del CNR, 56124 Pisa, Italy

<sup>7</sup> Department of Mechanical Engineering, The University of Hong Kong, Hong Kong Special Administrative Region of China, People's Republic of China

<sup>8</sup> School of Environment Science and Spatial Informatics, China University of Mining and Technology, Xuzhou, People's Republic of China

<sup>9</sup> Department of Atmospheric & Environmental Sciences, Gangneung-Wonju National University, Gangneung, Republic of Korea

<sup>10</sup> Department of Civil and Environmental Engineering, Yonsei University, Seoul, Republic of Korea

\* Author to whom any correspondence should be addressed.

E-mail: [flex.zhu@polyu.edu.hk](mailto:flex.zhu@polyu.edu.hk)

**Keywords:** NO<sub>2</sub>, air quality, COVID-19, lockdowns, urban mobility

## Abstract

The massive lockdown of global cities during the COVID-19 pandemic is substantially improving the atmospheric environment, which for the first time, urban mobility is virtually reduced to zero, and it is then possible to establish a baseline for air quality. By comparing these values with pre-COVID-19 data, it is possible to infer the likely effect of urban mobility and spatial configuration on the air quality. In the present study, a time-series prediction model is enhanced to estimate the nationwide NO<sub>2</sub> concentrations before and during the lockdown measures in the United States, and 54 cities are included in the study. The prediction generates a notable NO<sub>2</sub> difference between the observations if the lockdown is not considered, and the changes in urban mobility can explain the difference. It is found that the changes in urban mobility associated with various road textures have a significant impact on NO<sub>2</sub> dispersion in different types of climates.

## 1. Introduction

In December 2019, the pandemic outbreak of severe acute respiratory syndrome coronavirus 2 (SARS-CoV-2) emerged in Wuhan, China, after which more than 10 million cases are confirmed and 500 000 deaths are resulted by 1 July 2020, and the pandemic also spread in over 250 countries in the world. Despite the progressive increase in the number of confirmed cases every day, the situation has become relatively stable in some countries after the massive lockdown is adopted and strict travel control

measures are taken since March 2020 (Kucharski *et al* 2020). Due to the global lockdown, the *coronavirus disease 2019* (COVID-19) has undermined worldwide economies and triggered a global crisis due to great loss in the socioeconomic domain described by the United Nations (UNnews 2020). It was predicted that global trade will decline by 13%–32% and the annual global gross product is projected to decline by 24% (CRS 2020). Additionally, a strict lockdown in China reduced global GDP by 3.5% and Chinese GDP by 21% (Guan *et al* 2020). Notwithstanding, the socioeconomic is chronically and devastatingly hit by

the disease, and the environment has responded to the pandemic instantly (Fan *et al* 2020). The level of nitrogen dioxide ( $\text{NO}_2$ ) is substantially reduced in the wake of COVID-19 (Mahato *et al* 2019). In Central China,  $\text{NO}_2$  emission is decreased by 30% on a year-after-year basis during the Lunar New Year compared with the period from 2005–2019 (Earth Observatory 2020). The reduction of air pollution including  $\text{NO}_2$  is first identified appeared in Wuhan, and such phenomena are found in more and more cities and countries, and eventually it becomes a worldwide phenomenon (Venter *et al* 2020). Among 31 major cities in the world, a significant decline in  $\text{NO}_2$  has been observed in almost two-thirds of the study area after the lockdown, including New York, Rome and Paris, implying that the transportation and anthropogenic activities in the cities mentioned above were massively lessened (Shrestha *et al* 2020). Epidemiological evidence suggested that the high incidence of respiratory disease and many death tolls should be attributed to the deteriorated air quality (Brauer *et al* 2010). For example, approximately 4.6 million individuals died from the disease annually due to the low air quality, as reported by the World Trade Organisation (Cohen *et al* 2017), and the lung tissue can be damaged by prolonged exposure to  $\text{NO}_2$ , which is one of the contributors to the morbidity of asthma and lung cancer (Greenberg *et al* 2016, Khaniabadi *et al* 2017). Thus, it is of great significance to the enhancement of the atmospheric environment by grasping the evolutionary patterns of  $\text{NO}_2$  and its causal factors appropriately (He *et al* 2020).

Road traffic can be regarded as the major contributor to  $\text{NO}_2$  (Palmgren *et al* 2007, Keulen *et al* 2009, Mohegh *et al* 2020). The rise of  $\text{NO}_2$  concentration might cause a certain type of diesel particulate produced by heavy vehicles such as buses, whereas nitrogen is produced by the gasoline-fuelled passenger cars, particularly sensitive to long-range transport decomposition (Carslaw *et al* 2005, Heeb *et al* 2008). According to an observation of the vehicle emission factors, it is found that the decreasing trend of  $\text{NO}_2$  emission is the smallest and insignificant among other pollutants throughout the 12 years study period in Switzerland (Hueglin *et al* 2006), which suggests that the road traffic emission ratio in  $\text{NO}_2$  increased during this period. A similar outcome means that  $\text{NO}_2$  from the traffic emission is the key factor for generating ambient  $\text{NO}_2$  concentration (Kurtenbach *et al* 2012). As such,  $\text{NO}_2$  concentration will not be reduced substantially if only the  $\text{NO}_x$  exhaust system is improved without a significant reduction of traffic-related  $\text{NO}_2$  emission. It is found that  $\text{NO}_2$  had diurnal and seasonal variation as a function of traffic volumes alongside a major arterial (Kendrick *et al* 2015) and the traffic signals were related to the roadside air quality in Tokyo (Minoura *et al* 2010). Some studies also found that the change in  $\text{NO}_2$  concentration is highly dependent on the traffic capacity

and fuel decomposition, as well as the vehicle speed and fleet composition (Tang *et al* 2019). Nevertheless, it is reckoned that the improved air quality is mainly a result of the favourable meteorological conditions rather than the minimized anthropogenic activities because the pollutant diffusivity was an important factor closely related to meteorology (Wang *et al* 2020).

Another factor that contributes to  $\text{NO}_2$  emission is traffic characteristics. By investigating the correlation between  $\text{NO}_2$  and its emission factor, researchers speculated that the deviation of the contributing factors  $\text{NO}_2$  emission resulted from the variability of the local road condition, the traffic pattern and the fleet composition (Chan *et al* 2004, Liu *et al* 2012). The road 300 km or above in length was featured by higher  $\text{NO}_2$  concentration as shown by a study conducted in the Netherland (Velders *et al* 2009), and the study result is consistent with another finding that a higher  $\text{NO}_2$  exposure was associated with the road length variability in Shanghai (Meng *et al* 2015). Moreover, the spatial distribution and the local variability of  $\text{NO}_2$  concentration (Wang *et al* 2020) are analytically explored, and the results show that the local variation was mostly driven by regional differences between the ten most urbanized areas in the United States, which was consistent with the basic conditions of these urban regions, that is, comparatively denser traffic and frequent anthropogenic emission. Therefore, different spatio-temporal locations and the traffic characteristics have a significant influence on the level of  $\text{NO}_2$ , even though some of the emission features result from specific industrial activities. In the US metropolitan cities, the local  $\text{NO}_2$  concentrations can be improved by reducing the road traffic even if there is a variability of estimation error in  $\text{NO}_2$ . Therefore, no effective prediction model has been developed for national  $\text{NO}_2$  concentration yet (Lee *et al* 2019).

As a reliable and accurate method for mathematical modelling, auto-regressive integrated moving average (ARIMA) has been widely applied to short-term time-series trend analysis and its frequent application in the prediction from multiple perspectives. For instance, it was adopted in the study trying to make an accurate forecast of wind speed at wind power plants and ensure the overall stability and security of the power system (Singh *et al* 2019). Likewise, the time-series trend is explored to predict the capacity of electricity generation (Haiges *et al* 2017). In other disciplines, the statistical tool was adopted to detect financial crisis events that act as the precursor of the market regime (Faranda *et al* 2015). Apart from the modelling platform of geographic information systems (GIS) for spatial clustering and statistical analysis, the spatial distribution and the association between infectious diseases and  $\text{NO}_2$ , and between the traffic flow and the number of people moving trajectory are also identified (Yongjian *et al* 2020).

The assessment of the traffic related-GIS parameters such as the lengths of the major road segment and the traffic intensity can help reveal the long-term trend of NO<sub>2</sub> and their emission ratio related to the road traffic activities, and the impact on NO<sub>2</sub> can be visualized using the GIS platform (Shon *et al* 2011). With the use of predictive data based on ARIMA, the spatial transmissions of the pandemic disease can be forecasted regarding the spatial allocation of medical resources and the implementation of mitigating control measures (Lakhani 2020, Singer *et al* 2020).

This paper is organized as follows. Section 2 enhances a time-series prediction model to predict NO<sub>2</sub> concentrations accurately and proposes four indices to present the characteristics of road networks. Section 3 introduces data collection, presents the changes of NO<sub>2</sub> concentration after lockdown, and explores the impacts of road networks and regional climates on NO<sub>2</sub> concentration. Finally, section 4 makes a discussion and conclusion.

## 2. Methods

### 2.1. NO<sub>2</sub> difference between observation and prediction

The NO<sub>2</sub> concentration records before lockdown will be used to train historical patterns that contain seasonal and cyclic time-series information, and the SARIMAX model will be used to predict the NO<sub>2</sub> concentration. In this case, a prediction following historical patterns will not integrate with the new evolution after lockdown measures. Under the circumstance, two definitions are proposed to investigate the evolution:

- NO<sub>2</sub> difference denoted by  $\Delta d$  calculates the difference between the observed and predicted NO<sub>2</sub> concentration at a station after lockdown; and
- NO<sub>2</sub> change denoted by  $\Delta c$  calculates the difference of the mean NO<sub>2</sub> concentration before lockdown and that after lockdown based on observation or prediction.

Particularly,  $\Delta d$  can be significant as a result of the changes of urban mobility during the implementation of lockdown measures. Thus, we can investigate the relationship between  $\Delta d$  and the changes of urban mobility ( $\Delta m$ ) subject to a baseline before lockdown.

### 2.2. Seasonal autoregressive integrated moving average with eXogenous factors (SARIMAX)

The general ARIMA model consists of three parts, namely autoregression (AR), differencing (I) and moving average (MA), and the model can be presented as follows:

$$\text{ARIMA}(p, d, q), \quad (1)$$

where  $p$  denotes the order of auto-regressive model,  $d$  represents the order of difference, and  $q$  is the order

of moving average model. Nonetheless, seasonal patterns cannot be established by introducing an ordinary ARIMA model. To address this problem, the seasonal auto-regressive integrated moving average (SARIMA) includes the seasonal parameters for the auto-regressive, differencing and moving average terms, and the time step for modelling the periodic time-series pattern:

$$\text{ARIMA}(p, d, q)(P, D, Q)_t, \quad (2)$$

where  $P$  denotes the order of seasonal auto-regressive model,  $D$  denotes the order of seasonal differencing,  $Q$  is the order of seasonal moving average model, and  $t$  refers to the time step parameter for seasonality. Furthermore, Seasonal Autoregressive Integrated Moving Average with eXogenous factors (SARIMAX) can be used to analyse the time-series data with additional variables in the regression operation (Valipour 2015):

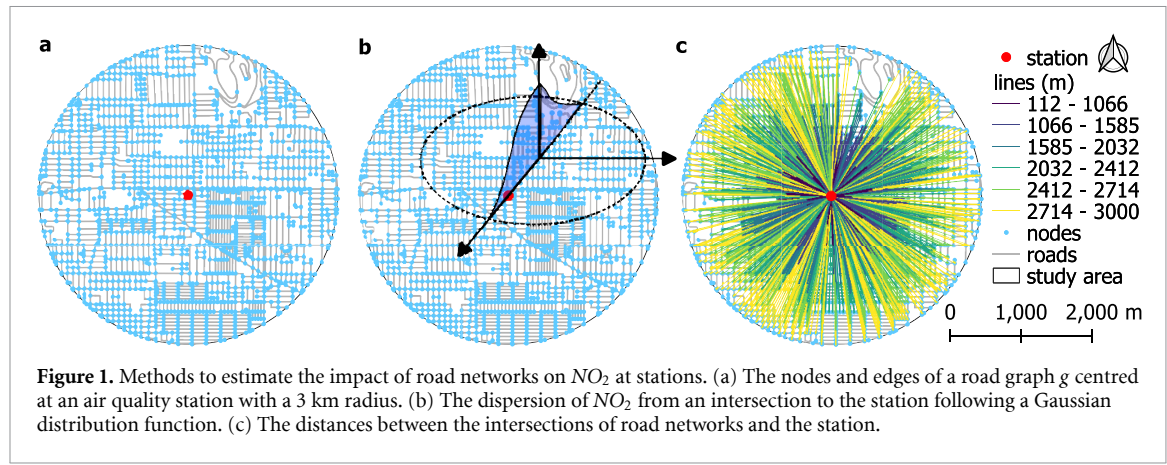
$$\text{ARIMAX}(p, d, q)(P, D, Q)_t. \quad (3)$$

In this study, the time-series NO<sub>2</sub> measurements of 56 stations in the US were modelled using the SARIMAX model based on the exogenous weather variables including air temperature, air pressure, relative humidity, wind speed and percentage of cloud coverage. Since there might be more than one seasonal pattern for the time-series NO<sub>2</sub> data, six Fourier series with different periods were also included as exogenous variables (number of days = {15, 30, 90, 180, 365}), and 7 days (one week) was deemed to be the seasonal time step  $t$  in the SARIMAX model.

Before the SARIMAX modelling is performed, the randomness and normality were tested with Ljung–Box test and Jarque–Bera test. The Augmented Dickey–Fuller test and the Osborn, Chui, Smith, and Birchenhall tests were performed to determine the seasonally varying parameters ( $d$  and  $D$ ) of the time series respectively. Canova-Hansen test was conducted to determine the time step parameter ( $t$ ) for seasonality. Then, a stepwise approach (Hyndman *et al* 2008) was adopted for optimizing the other parameters (i.e.  $p$ ,  $q$ ,  $P$ , and  $Q$ ) of the SARIMA model by minimizing the Akaike information criterion (AIC) value. The optimized parameters were introduced for the NO<sub>2</sub> prediction in this study. Python 3.7 and the *statsmodels* package (State Space Methods 2020) were used for training and prediction.

### 2.3. Impacts of road networks on vehicle emission

As traffic is one of the major sources of NO<sub>2</sub>, in the present study, four indices are adopted to explain the characteristics of road networks in a 3 km-radius circular area centred at each air quality monitoring station (figure 1(a)), which are used for correlation analysis between NO<sub>2</sub> difference after lockdown. The four indices are enumerated as follows:



(1)  $n_{nd}$  denotes the number of road intersections, (2)  $c_{nd}$  presents the number of the road segments at all the intersections, (3)  $s_{rd}$  stands for the total length of the road networks, and (4)  $n_{rd}$  is the number of the road segments. It is crucial for proposing  $n_{nd}$  since vehicles often stop at the intersections because of the traffic lights, which leads to the accumulation of a considerable amount of the emissions during idling (Minoura *et al* 2010). In comparison,  $c_{nd}$  shall be more representative than  $n_{nd}$  because the number of roads connecting at each intersection is counted that may indicate temporary stopping more confidently. For example, vehicles are more likely to be parked at an intersection of two roads than a single road with the same traffic volume.  $s_{rd}$  also plays a big part since it affects traffic flows fundamentally. The four indices are thus organized as  $i = \{n_{nd}, c_{nd}, s_{rd}, n_{rd}\}$ . In the study,  $G$  denote a topological graph of roads that edges  $E = \{e\}$  connect with each other by associating with the nodes  $O = \{o\}$ , getting  $G = \{E, O\}$ . Notably,  $n_{nd}$  is different from the number of nodes denotes by  $\text{num}(O)$  because only two edges connecting through a node means they are the same road essentially, which is caused by the data format. Thus,  $n_{nd}$  and  $c_{nd}$  are counted when a node at least associates with at least edges.

However, based on the four indices, it is estimated that the dispersion of vehicle emissions at road networks has homogeneous impacts on stations' air quality when the spatial distance between them is taken into consideration. To make a better estimation, in the present study, it is assumed that the dispersion of each index follows a Gaussian distribution from each element of the index to the station (figure 1(b), equation (4)):

$$y = y_0 + Ae^{-\frac{(x-x_c)^2}{2w^2}}. \quad (4)$$

In the function,  $y_0$  denotes the offset and  $x_c$  is the centre, both equalling 0 to present a normalized Gaussian.  $A$  is the *amplitude* to denote the magnitude of the element,  $w$  implies the *width* to control the speed of the dispersion, and  $x$  stands for the distance

from the element to the station (figure 1(c)). When computing  $n_{rd}$  and  $s_{rd}$  enriched with the Gaussian function,  $x$  is the distance from the middle point of the road segment to the station, as an approximation. Then, the total impacts of all the elements of an index at a station can be accumulated (equation (5)):

$$Y = \sum_{m=1}^n y = \sum_{m=1}^n g(A_m, x_m, w). \quad (5)$$

A set of abbreviations and their definitions are summarized in table 2 for clear presentation of this study.

## 2.4. Data

Daily  $\text{NO}_2$  observations at 56 stations in 54 cities across the US are derived from the *Air Quality Open Data Platform* during a period from June 2014 to May 2020 (AQODP 2020), which are complemented by the geographical coordinates. The weather data taken as exogenous factors in the SARIMAX model are collected from OpenWeatherMap (Open Weather 2020) with the coordinates of the 56  $\text{NO}_2$  stations. The *COVID-19 Community Mobility Reports* from Google provides *daily* mobility changes in percentage subject to the baseline on 15 February 2020 (Google 2020), indicating user mobility in Google Maps during the COVID-19 pandemic. Mobility is aggregated and anonymized as six categorical purposes, including retail and recreation, groceries and pharmacies, parks, transit stations, workplaces, and residences. The originally collected  $\text{NO}_2$  data and the mobility data have the same temporal resolution on one day, so that preprocessing is not needed. The study is based on the data collection between 15 February 2020 and 6 May 2020, which is the last day of the  $\text{NO}_2$  data. Road networks in the US are acquired from OpenStreetMap (2020).

## 3. Results

### 3.1. $\text{NO}_2$ change after lockdown

Figure 2 presents 56  $\text{NO}_2$  stations in the US, covering a large geographical space, and table 1 summarizes

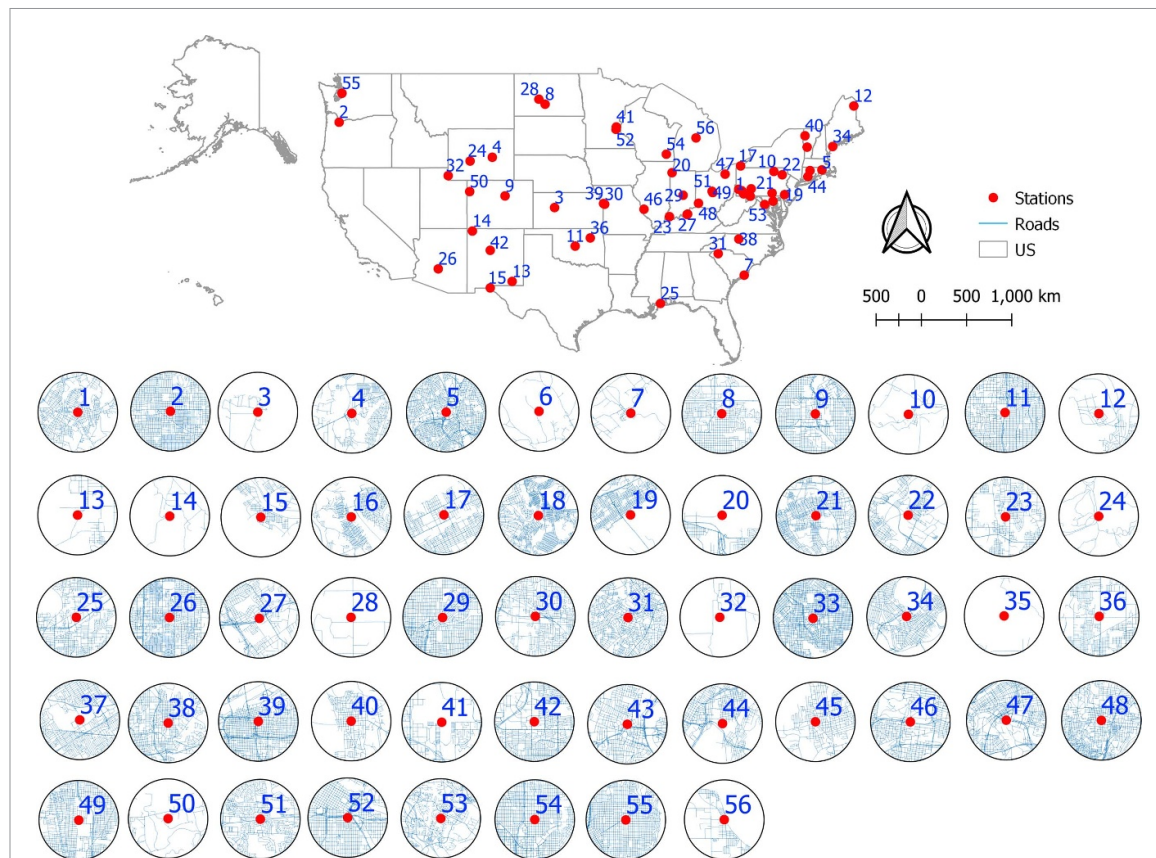


**Figure 2.** Locations of 56 air quality stations across the United States. Each circular area has a 3 km radius centred at the stations, which are presented as the red dots with IDs. The densities of the road networks are diverse across the whole area.

**Table 1.** The station IDs are listed in six different climate types.

No.	Climate	Station ID
1	Costal	5, 7, 19, 20, 25, 33, 34, 44, 53–55
2	Inland	1–4, 6, 8–18, 21–24, 26–32, 35–52, 56
3	Arid	3, 4, 8, 9, 11, 13–15, 24, 26, 28, 32, 42, 50
4	Humid	1–2, 5–7, 10, 12, 16–23, 25, 27, 29–31, 33–41, 43–49, 51–56
5	Hot	1–3, 5–7, 10, 11, 13–23, 25–27, 29–31, 33, 35–39, 42–44, 46–49, 51, 53, 55
6	Cold	4, 8, 9, 12, 24, 28, 32, 34, 40, 41, 45, 50, 52, 54, 56

six climate types that prevail at the stations according to National Weather Service (2020). The stations are located in various micro-environments with different road networks, and they are located in urban or rural areas of those cities that implement lockdown when the COVID-19 pandemic becomes quite severe. The training has been done at each station since June 2014. Then, the SARIMAX model is used to predict *daily* NO<sub>2</sub> at each station from the start of lockdown to the end of lockdown.

Two predictions are made, with one prediction period starting 60 days ( $n = 60$ ) before the lockdown and ending a number of days after the lockdown (until 6 May 2020), and the other prediction period is starting 30 days ( $n = 30$ ) before the lockdown and

**Table 2.** Definitions of the abbreviations used in this study.

No.	Abbre.	Definition
1	$\Delta d$	NO <sub>2</sub> difference: the predicted NO <sub>2</sub> concentration minus the observed NO <sub>2</sub> concentration at a station after lockdown
2	$e$	relative error: $\Delta d$ divided by the observed NO <sub>2</sub> concentration
3	$\Delta c$	NO <sub>2</sub> change: the mean NO <sub>2</sub> concentration after lockdown minus that before lockdown
4	$\Delta c_p$	NO <sub>2</sub> change in percentage: $\Delta c$ divided by the mean NO <sub>2</sub> concentration before lockdown
5	$\Delta m$	the mean change of urban mobility subject to a specific day before lockdown; $\{\Delta m_w, \Delta m_r, \Delta m_t\}$ are the changes of mobility for <i>workplace</i> , <i>recreation</i> , and <i>public transit</i>
6	$n_{nd}$	the number of road intersections
7	$c_{nd}$	the number of the road segments connecting at all the intersections
8	$s_{rd}$	the total length of the road networks
9	$n_{rd}$	the number of the road segments
10	$\Delta m_{rd}$	$\Delta m_{rd} = s_{rd} \cdot \Delta m_w$

ending a number of days after the lockdown. Figure 3 visualizes prediction results of two selected sites that the red curves (observation) present a seasonal and periodical pattern, which are lower than the blue

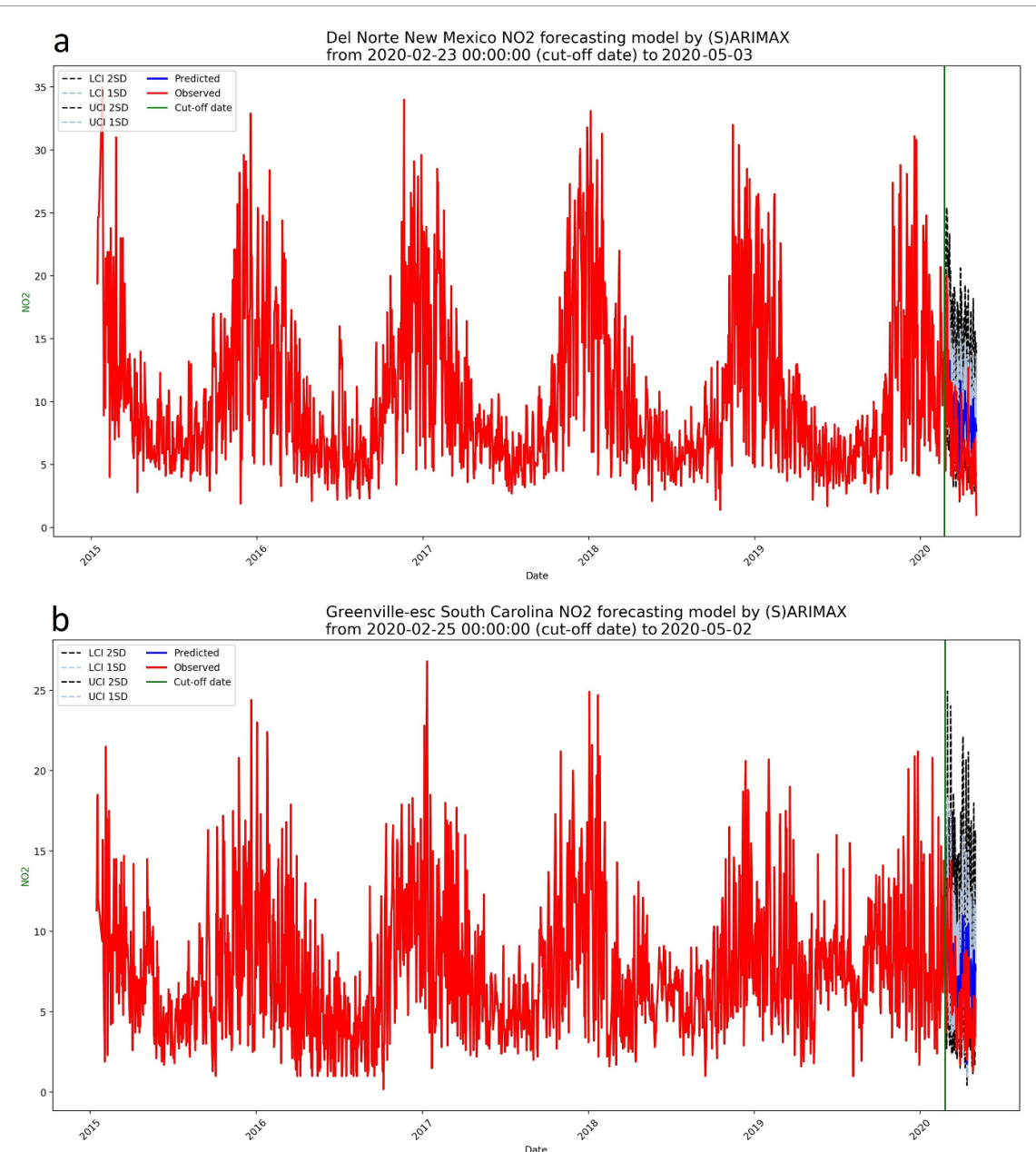


**Figure 3.** Prediction of the two selected sites. (a) Site located at Del Norte, New Mexico. (b) Site located at Greenville, South Carolina.

curves (prediction). The difference between the blue and red curves (i.e. NO<sub>2</sub> difference) confirms our hypothesis that the prediction has not incorporated the disruption of lockdown and can be explained by the reduction of mobility.

Figure 4(a) provides the distribution of the *mean* relative errors ( $e$ ) of the prediction at all the stations. Evidently, the errors before lockdown ( $b$ ) are smaller than after lockdown ( $a$ ), with the medians at  $e = 0.13$  for  $n = 60$  and  $e = 0.12$  for  $n = 30$ , respectively. It suggests that satisfactory prediction accuracy is achieved prior to the lockdown accordingly. When the lockdown was activated, the medians become larger at  $e = 0.22$  for  $n = 60$  and  $e = 0.20$  for  $n = 30$ , which indicates that it is challenging to obtain accurate prediction caused by disruptive lockdown measures.

Besides, both errors for  $n = 30$  are slightly smaller than that for  $n = 60$ , probably because  $n = 60$  has a longer prediction time while  $n = 30$  allows an additional 30 day training that better incorporates the most recently seasonal variation into the prediction.

To probe into the impact of the lockdown measures, in the present study, the NO<sub>2</sub> changes before and after lockdown for the 56 stations based on prediction ( $p$ ) and observation ( $o$ ) are calculated, respectively. It is found that many stations have undergone a substantial reduction after lockdown in view of the changes of absolute values ( $\Delta c$ ) (figure 4(b)), which become more significant when conversion into percentages that  $\Delta c_p$  equals  $\Delta c$  divided by the mean concentration before lockdown (figure 4(c)). Specifically, the observation suggests

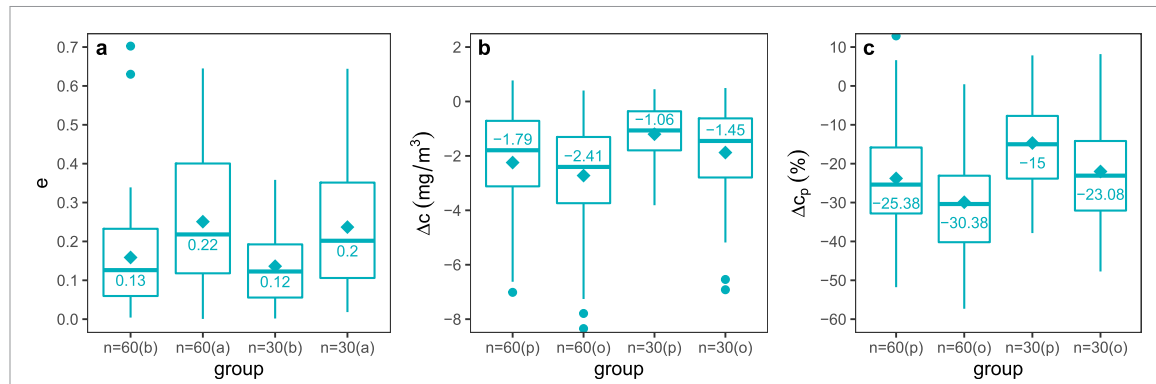
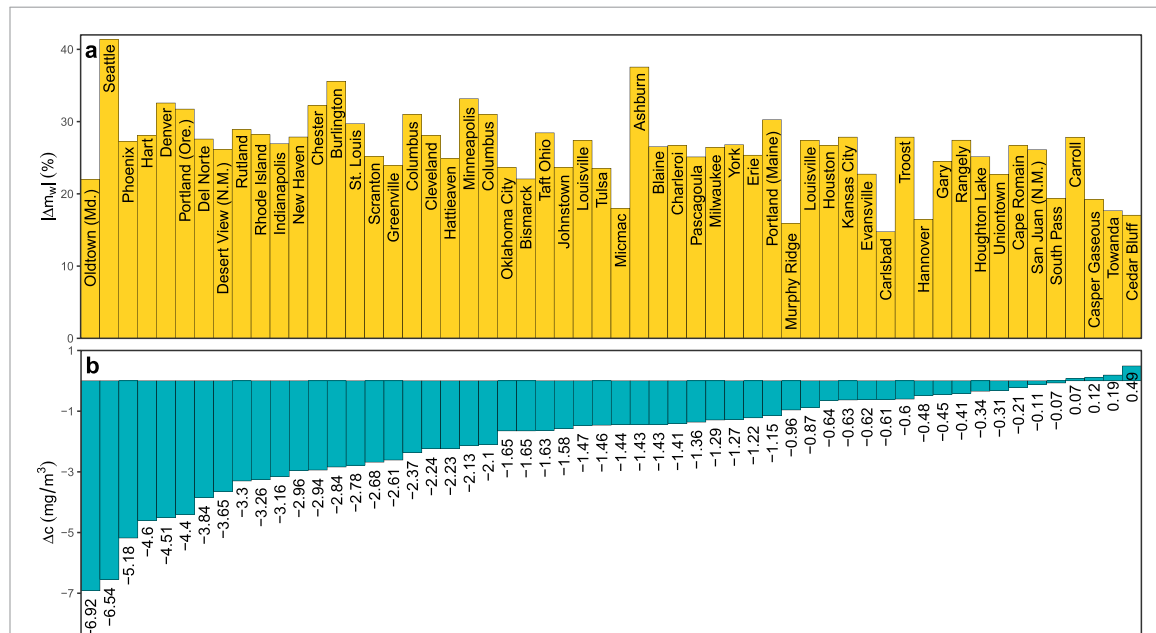


**Figure 4.** Relative errors of NO<sub>2</sub> prediction and statistics of NO<sub>2</sub> change. The numbers in each plot are the medians of statistics at the 50th percentile. The training has been implemented since 2014 at each station and the two predictions start from 60 days ( $n = 60$ ) and 30 days ( $n = 30$ ) before the lockdown dates. (a) Relative errors of the predicted NO<sub>2</sub> concentrations ( $e$ ) at the 56 stations respectively before (b) and after (a) lockdown. (b) NO<sub>2</sub> changes ( $\Delta c$ ) obtained from prediction ( $p$ ) and observation ( $o$ ). (c) NO<sub>2</sub> changes in percentage ( $\Delta c_p$ ) obtained from prediction ( $p$ ) and observation ( $o$ ).



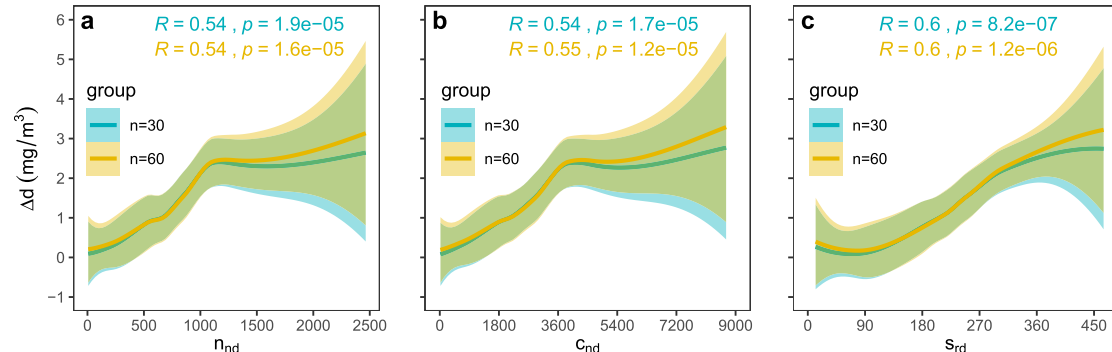
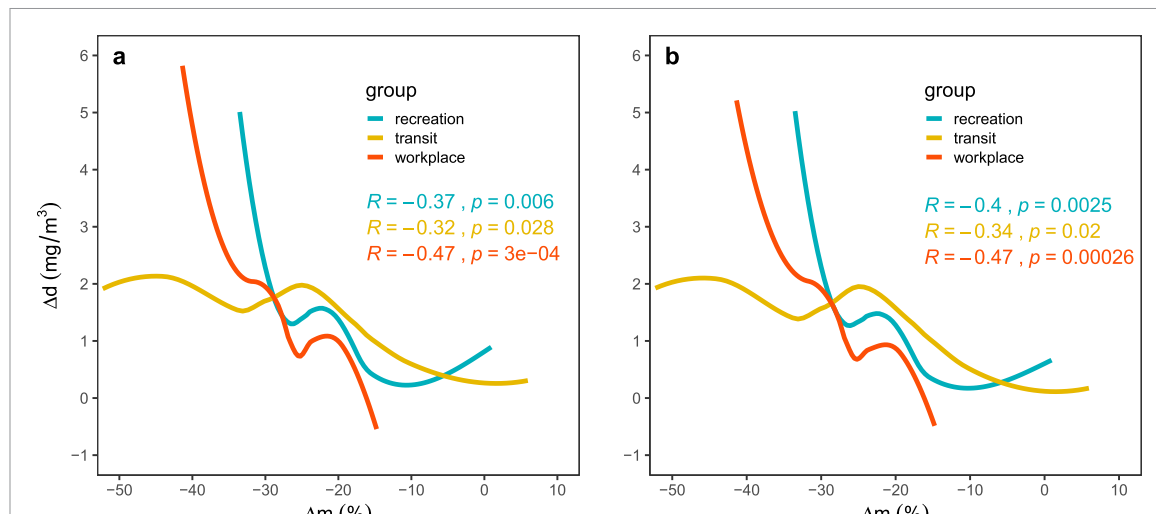
that half of the NO<sub>2</sub> measurements decreased at least with  $-1.45 \text{ mg m}^{-3}$  for  $n = 30$  and  $-2.41 \text{ mg m}^{-3}$  for  $n = 60$  (figure 4(b)), which is equivalent to a 23.08% and 30.38% reduction of the NO<sub>2</sub> concentration before lockdown. Meanwhile, the predicted number is slightly larger than the observation.

According to the *COVID-19 Community Mobility Reports* from Google that provides relative urban mobility subject to a baseline before lockdown in each city, all the involved cities have shown a huge decrease in the mobility for *workplace* with  $|\Delta m_w| > 20\%$ , in which Seattle, Ashburn, Burlington, and Minneapolis have witnessed the largest reduction with  $|\Delta m_w|$  equalling 41%, 38%, 36%, and 33%, respectively (figure 5(a)). By inspecting each station, the observation suggests that a considerable reduction of NO<sub>2</sub> after lockdown is realized in most cities, while a

tiny increase is found in four cities quite unexpectedly (figure 5(b)). Notably, the changing trend of  $|\Delta m_w|$  is unclear with the decrease of  $\Delta c$ , which stimulates our motivation to explore the influential factors.

### 3.2. Association between urban mobility and NO<sub>2</sub> difference

Considering the vehicle emission is one of the largest resources of NO<sub>2</sub>, a significant reduction of urban mobility during the pandemic is supposed to have impacts on the changes of NO<sub>2</sub> in cities, which focuses on a detailed investigation by contrast with other studies at regional and national scales. Based on the *COVID-19 Community Mobility Reports*, the Pearson correlation analysis between the NO<sub>2</sub> difference ( $\Delta d$ ) and the *averaged* mobility changes ( $\Delta m$ ) is made, in categories of  $n = 30$  (figure 6(a)) and



$n = 60$  (figure 6(b)). It shows that the mobility for *workplace* decreases significantly in all cities ( $-40\% \leq \Delta m_w \leq -15\%$ ), which validates a moderate and negative correlation with  $\Delta d$  in both groups (the Pearson correlation coefficient  $R = -0.47, p < 0.05$ ). Similarly, the mobility for *recreation* has shown a considerable decrease in a vast majority cities ( $-30\% \leq \Delta m_c \leq 1\%$ ), having a weak and negative correlation with  $\Delta d$  ( $R = -0.37$  for  $n = 30$  and  $R = -0.40$  for  $n = 60$ ). In comparison, the greatest decrease in *transit* mobility is observed in almost all the cities ( $-50\% \leq \Delta m_t \leq 5\%$ ), which contributes to a weak and negative correlation ( $R = -0.32$  for  $n = 30$  and  $R = -0.34$  for  $n = 60$ ) (figure 6).

As an expectation, a small increase of  $\Delta m_c = 0.94\%$  and  $\Delta m_c = 5.95\%$  is revealed in the *recreation* mobility for the Cedar Bluff State Park in Kansas and the *transit* mobility for Murphy Ridge in Wyoming, respectively. It is reasonable since some populations may deliberately choose not to travel to crowded locations and move to rural areas as temporary residences such as parks. Three implications can also be induced by the results. Firstly, the lockdown policy

helps reduce urban mobility for *recreation*, *transit*, and *workplace* greatly during the pandemic, leading to a considerable reduction of  $\text{NO}_2$ . Secondly, the correlations between  $\Delta m$  and  $\Delta d$ , even though not robustly significant, suggest the validation of the hypothesis that the difference of  $\text{NO}_2$  has resulted from the changes in urban mobility. Last but not least, other factors such as road characteristics or local climates may also affect the changes of  $\text{NO}_2$  since the current correlations are not significantly strong.

### 3.3. Impacts of road networks on $\text{NO}_2$ concentration

As the urban mobility restraint by road networks, in the present studies, it is proposed that the road characteristics, such as the density of road networks, may have notable impacts on emission. Therefore, three static indices are put forth to represent road characteristics  $i = \{n_{nd}, c_{nd}, s_{rd}\}$ : (1) the number of road intersections  $n_{nd}$ , (2) the total number of the road segments connecting at all the intersections  $c_{nd}$ , and (3) the total length of the road networks  $s_{rd}$ . Figure 7 demonstrates the correlations between

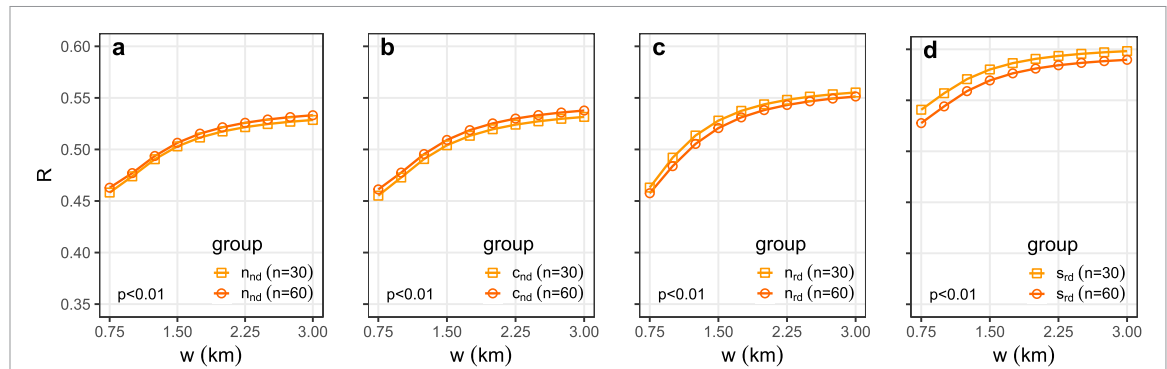


**Figure 8.** Pearson correlation coefficient ( $R$ ) between the four indices of road networks ( $c_{nd}$ ,  $n_{nd}$ ,  $s_{rd}$ ,  $n_{rd}$ ) and  $\Delta d$ .  $w$  in the  $x$ -axis represents the width of the Gaussian function used to estimate the impact of the four indices on weather stations, and  $R$  in the  $y$ -axis has  $p \leq 0.01$ . (a)–(d) Correlations are based on  $n = 30$  and  $n = 60$ .

$i$  and  $\Delta d$ , categorizing into two groups of  $n = 30$  and  $n = 60$ . It is pointed out that both groups obtain somewhat strong and positive correlations that the coefficients  $R = \{0.54, 0.54, 0.60\}$  for  $n = 30$ , resulting a better performance than  $(\Delta m, \Delta d)$  in figure 6. It can be explained that a larger indicator in  $i$  makes a more significant effect on the changes of  $\text{NO}_2$  after lockdown, suggesting that road networks' characteristics can greatly affect  $\Delta d$ . However, the three indicators treat intersections and roads with homogeneous impacts on the air quality stations, regardless of the spatial distance between the roads and stations.

To make the indices more representative, we used a Gaussian function  $y = \sum g(A, x, w)$  to estimate the dispersion of  $\text{NO}_2$  from the vehicle emission, in which  $A$  represents the magnitude of the road property,  $x$  denotes the distance from roads to the  $\text{NO}_2$  station, and  $w$  indicates the width of the function. In addition, another road index named  $n_{rd}$  is initiated, which means that the dispersion associated with the road follows the Gaussian distribution but ignoring the characteristics of the road length to compare with the performance of  $s_{rd}$ . Figure 8 shows the coefficient curves between  $i = \{n_{nd}, c_{nd}, s_{rd}, n_{rd}\}$  and  $\Delta d$ , comparing between  $n = 30$  and  $n = 60$ . Overall, all the curves grow steadily and approach the upper bounds gradually with an increase of  $w$ . Particularly,  $c_{nd}$  and  $n_{nd}$  share the same growing trend with the increase of  $w$  that their  $R_{\max} < 0.55$  (figures 8(a) and (b)). Also,  $c_{nd}$  is insignificantly larger than  $n_{nd}$  with the same  $w$  and the same group  $n = 30$  or  $n = 60$ . Comparatively,  $s_{rd}$  and  $n_{rd}$  perform better than  $c_{nd}$  and  $n_{nd}$  regarding the correlation coefficients  $R$ . Meanwhile,  $s_{rd}$  overtakes  $n_{rd}$  notably for both  $n = 30$  and  $n = 60$ , and  $s_{rd}$  shows the most prominent correlation with  $R_{\max} \approx 0.60$  when  $w = 3$  km (figures 8(c) and (d)). Two phenomena can be observed from the figure. On the one hand,  $s_{rd}$  obtains the strongest impact on  $\Delta d$ , which is convincing since  $s_{rd}$  incorporates the  $\text{NO}_2$  source from roads and  $\text{NO}_2$  dispersion following the Gaussian distribution into the correlation. For instance, a long road is likely to produce more  $\text{NO}_2$

while a short distance to the station is related to a greater amount of  $\text{NO}_2$ . On the other hand,  $w = 2.25$  km is an empirical distance that road networks start to have a rather weak impact on  $\Delta d$ .

### 3.4. Impacts of regional climates on $\text{NO}_2$ concentration

The present study considers that regional climates can also affect the dispersion of  $\text{NO}_2$ . It is based on the evidence that air temperatures were used to describe urban heat islands and climate largely determines the magnitude of urban heat islands (Zhao *et al* 2014, Manoli *et al* 2019). As both air temperatures and  $\text{NO}_2$  are air properties essentially,  $\text{NO}_2$  concentrations may also be influenced by climate. To explore the combined impacts of urban mobility and road networks in partition of different climates, the correlation analysis is performed in different climates, namely, *arid* and *humid* climates, *hot* and *cold* climates, and *coastal* and *inland* climates (figure 9(a)). The correlation analysis is performed between  $\Delta d$  and  $\Delta m_{rd} = s_{rd} \cdot \Delta m_w$ , where  $s_{rd}$  follows the Gaussian function with  $w = 3$  km that obtains the largest  $R$  and  $\Delta m_w$  is the change of workplace mobility as discussed in figure 6. Generally, results obtained from  $n = 30$  (figures 9(b)–(d)) and  $n = 60$  (figures 9(e)–(g)) are almost the same that  $(\Delta d, \Delta m_{rd})$  are strongly correlated. Particularly, the correlations are more prominent in the *arid*, *hot*, and *coastal* climates with  $R = \{-0.84, -0.65, -0.77\}$  than in the *humid*, *cold*, and *inland* climates, namely  $R = \{-0.60, -0.64, -0.64\}$  (figures 9(b)–(d)). In contrast, correlations based on  $n = 60$  are slightly weaker than  $n = 30$ . That is to say, the *arid*, *hot*, and *coastal* climates tend to facilitate the dispersion of  $\text{NO}_2$  based on a given urban mobility and road networks. It is also found that  $\Delta m_{rd}$  shows the most prominent correlation with  $\Delta d$ , and the significance of the correlations decreases from  $\Delta m_{rd}$  with the Gaussian distribution,  $s_{rd}$  with the Gaussian distribution (figure 8(d)),  $s_{rd}$  (figure 7(c)), to  $\Delta m_w$  (figure 6) when they are in the same condition. It suggests that the dynamic mobility constraint by static road

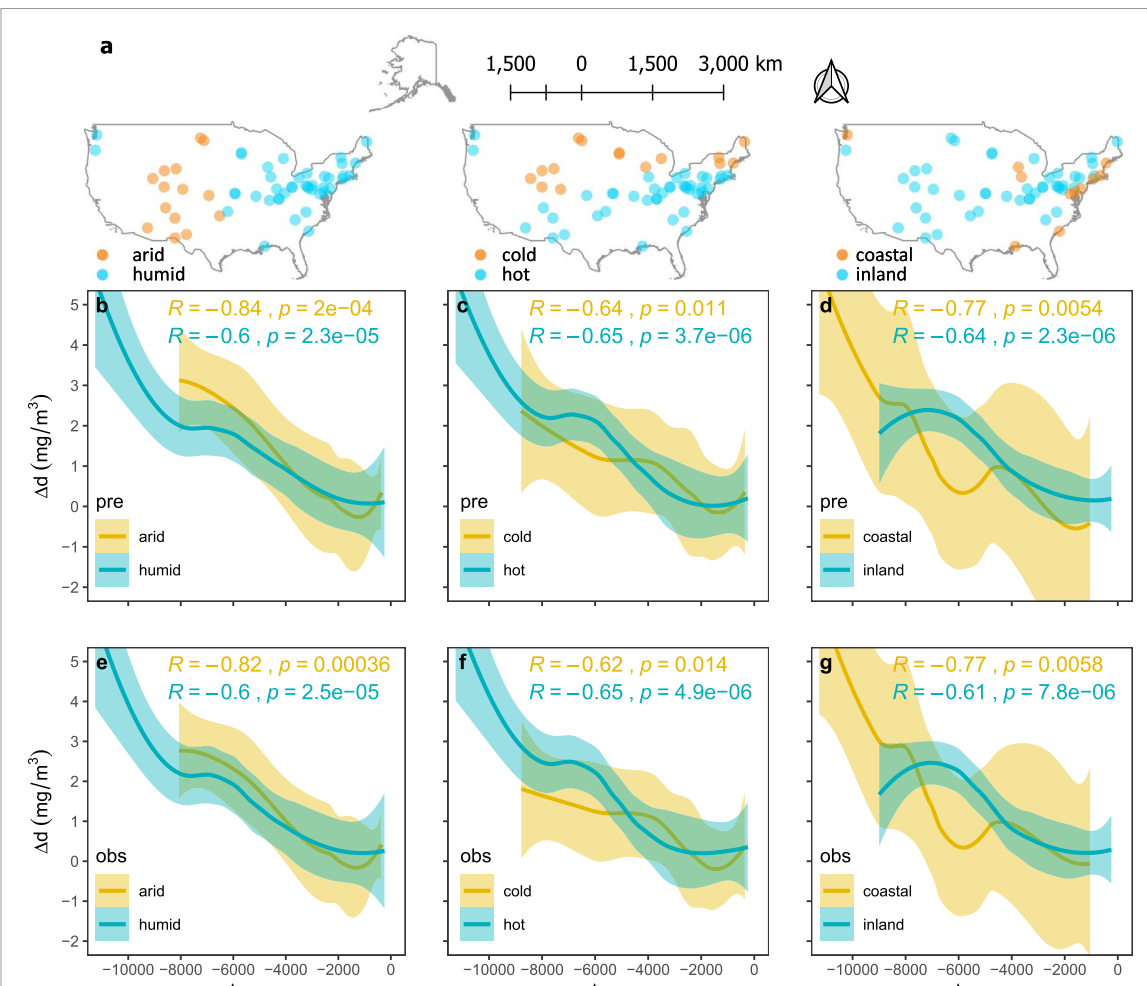


**Figure 9.** Pearson correlation coefficient ( $R$ ) between  $\Delta d$  and  $\Delta m_{rd}$  estimated by the Gaussian function ( $w = 3 \text{ km}$ ). The buffer areas symbolize the confidence intervals. (a) Stations are located at a place with six types of the climate. (b)–(d)  $R$  is derived from  $n = 30$ . (e)–(g)  $R$  obtained on the condition of  $n = 60$ . (b), (e) Stations are in the arid and humid climates. (c), (f) Stations are in the hot and cold climates. (d), (g) Stations are in the coastal and inland climates.

networks significantly affects the changes of NO<sub>2</sub> in a large geographical space.

#### 4. Discussion and conclusion

An accurate estimation of the time series of NO<sub>2</sub> is essential to predict and investigate the impact of the community mobility on the urban micro-environment. The study refines an established NO<sub>2</sub> prediction model and estimates the NO<sub>2</sub> concentrations without the disruption of COVID-19, which is achieved by incorporating the seasonal and cyclic variations based on years of historical data before 2020. Correlation analysis in this study is performed based on the hypothesis that the predicted level of NO<sub>2</sub> after lockdown is larger than the observed level because the lockdown policy leads to less frequent use of vehicles and thus less NO<sub>2</sub> emission while the prediction still follows historical patterns that have not incorporated the dramatic decrease of NO<sub>2</sub> after lockdown. Therefore, the changes of urban mobility have shown a causal relation with the difference of NO<sub>2</sub> concentrations between the prediction and

observation. The study also suggests that the proposed prediction and analysis method can be used to evaluate the environmental impacts when confronting the COVID-19 pandemic and other public health events.

The results suggest that part of the difference between predicted and observed values is the result of the disruptive lockdown measures. During the lockdown period, there are strong and negative correlations between  $\Delta d$  and  $\Delta m_{rd}$  in group of different climates because  $\Delta m_{rd}$  considers the changes of urban mobility, the total length of the roads, and the dispersion following a Gaussian distribution. Two major findings have been generalized as follows. Firstly, a great reduction of urban mobility associated with the *recreation*, *transit*, and *workplace* may result in a considerable decrease in NO<sub>2</sub> in a large geographical area. Secondly, the local climate is also one of the vital factors that have distinct impacts on the dispersion of NO<sub>2</sub>. Specifically, the impacts are more prominent for stations in areas where the arid, hot, and coastal climates prevail, since the three climates' correlations are considerably stronger. It is probably because the

arid and hot climates would cause uneven air temperatures, which promotes wind ventilation and reduces the NO<sub>2</sub> density, and it is also the case with coastal cities where there are wind cycles between the land and sea. Some features of local weather in terms of daily wind directions and strengths can also mitigate NO<sub>2</sub> concentrations.

The SARIMAX model considers meteorological conditions by establishing exogenous weather variables, such as wind speed and air pressure, optimized by minimizing the AIC value to achieve accurate prediction. Since this study aims to investigate the impacts of mobility on NO<sub>2</sub> concentration, we do not analyse the meteorological influence in detail. Alternatively, we have categorized the analysis into six climate types, which is used as background climate associating with meteorological conditions, to obtain generic phenomenon at a large geographical extent. The prediction with 30 and 60 days before lockdown suggests that instantly seasonal variation influences prediction accuracy, while their effect is insignificant when associating with mobility indicators to explain NO<sub>2</sub> concentration.

In conclusion, the proposed NO<sub>2</sub> difference between prediction and observation is an effective indicator to explain the improvement of the air quality after lockdown. The proposed  $\Delta m_{rd}$  can explain the NO<sub>2</sub> concentration comprehensively by considering the source of dynamic urban mobility, the spatial constraints of road networks, and physical dispersion process. The proposed analysis method can be used to investigate other air quality indicators and other disruptive infectious diseases.

## Data availability statement

The data that support the findings of this study are available upon reasonable request from the authors.

## Acknowledgments

Man Sing Wong thanks the funding support from a grant by the General Research Fund (Grant No. 15602619), and the Research Institute for Sustainable Urban Development (Grant No. 1-BBWD), the Hong Kong Polytechnic University. Mei-Po Kwan was supported by a grant from the Research Committee on Research Sustainability of Major RGC Funding Scheme of the Chinese University of Hong Kong. This research is supported by the National Research Foundation, Prime Minister's Office, Singapore under its Campus for Research Excellence and Technological Enterprise (CREATE) programme.

## ORCID iDs

Rui Zhu  <https://orcid.org/0000-0002-9965-0948>  
Coco Yin Tung Kwok  <https://orcid.org/0000-0001-6886-3281>

Kwon Ho Lee  <https://orcid.org/0000-0002-0844-5245>

## References

- Air Quality Open Data Platform 2020 Air pollution in world: real-time air quality index visual map (available at: <https://aqicn.org/map/world/>)
- Brauer M 2010 How much, how long, what and where: air pollution exposure assessment for epidemiologic studies of respiratory disease *Proc. American Thoracic Society* vol 7 pp 111–15
- Carslaw D C 2005 Evidence of an increasing NO<sub>2</sub>/NO<sub>x</sub> emissions ratio from road traffic emissions *Atmos. Environ.* **39** 4793–802
- Chan T L *et al* 2004 On-road remote sensing of petrol vehicle emissions measurement and emission factors estimation in Hong Kong *Atmos. Environ.* **38** 2055–66
- Cohen A J *et al* 2017 Estimates and 25-year trends of the global burden of disease attributable to ambient air pollution: an analysis of data from the global burden of diseases study 2015 *Lancet* **389** 1907–18
- Congressional Research Service 2020 Global economic effects of COVID-19 (available at: <https://fas.org/sgp/crs/row/R46270.pdf>)
- Earth Observatory 2020 Airborne nitrogen dioxide plummets (available at: <https://earthobservatory.nasa.gov/images/146362/airborne-nitrogen-dioxide-plummets-over-china>)
- Fan J L *et al* 2020 How do weather and climate change impact the COVID-19 pandemic? Evidence from the Chinese mainland *Environ. Res. Lett.* **16** 014026
- Faranda D *et al* 2015 Early warnings indicators of financial crises via auto regressive moving average models *Commun. Nonlinear Sci. Numer. Simul.* **29** 233–9
- Google 2020 COVID-19 community mobility reports (available at: <https://google.com/covid19/mobility/>)
- Greenberg N *et al* 2016 Different effects of long-term exposures to SO<sub>2</sub> and NO<sub>2</sub> air pollutants on asthma severity in young adults *J. Toxicol. Environ. Health A* **79** 342–51
- Guan D *et al* 2020 Global supply-chain effects of COVID-19 control measures *Nat. Hum. Mobility* **4** 557–87
- Haiges R, Wang Y D, Ghoshray A and Roskilly A P 2017 Forecasting electricity generation capacity in Malaysia: an auto regressive integrated moving average approach *Energy Proc.* **105** 3471–8
- He Q *et al* 2020 Spatially and temporally coherent reconstruction of tropospheric NO<sub>2</sub> over China combining OMI and GOME-2B measurements *Environ. Res. Lett.* **15** 125011
- Heeb N V, Saxer C J, Forss A M, Brühlmann S 2008 Trends of NO-, NO<sub>2</sub>- and NH<sub>3</sub>-emissions from gasoline-fueled Euro-3-to Euro-4-passenger cars *Atmos. Environ.* **42** 2543–54
- Hueglin C, Buchmann B and Weber R O 2006 Long-term observation of real-world road traffic emission factors on a motorway in Switzerland *Atmos. Environ.* **40** 3696–709
- Hyndman R J and Khandakar Y 2008 Automatic time series forecasting: the forecast package for R *J. Stat. Softw.* **27** 107590
- Kendrick C M, Koonce P and George L A 2015 Diurnal and seasonal variations of NO, NO<sub>2</sub> and PM<sub>2.5</sub> mass as a function of traffic volumes alongside an urban arterial *Atmos. Environ.* **122** 133–41
- Keukens M, Roemer M and van den Elshout S 2009 Trend analysis of urban NO<sub>2</sub> concentrations and the importance of direct NO<sub>2</sub> emissions versus ozone/NO<sub>x</sub> equilibrium *Atmos. Environ.* **43** 4780–3
- Khaniabadi Y O *et al* 2017 Exposure to PM<sub>10</sub>, NO<sub>2</sub> and O<sub>3</sub> and impacts on human health *Environ. Sci. Pollut. Res.* **24** 2781–9
- Kucharski A J, Russell T W, Diamond C, Liu Y and Edmunds J 2020 Early dynamics of transmission and control of

- COVID-19: a mathematical modelling study *Lancet Infectious Dis.* **20** 553–8
- Kurtenbach R, Kleffmann J, Niedojadlo A and Wiesen P 2012 Primary NO<sub>2</sub> emissions and their impact on air quality in traffic environments in Germany *Environ. Sci. Eur.* **24** 21
- Lakhani A 2020 Which Melbourne metropolitan areas are vulnerable to COVID-19 based on age, disability and access to health services? Using spatial analysis to identify service gaps and inform delivery *J. Pain Symptom Manage.* **60** 41–4
- Lee C 2019 Impacts of urban form on air quality in metropolitan areas in the United States *Comput. Environ. Urban Syst.* **77** 101362
- Liu L J S et al 2012 Long-term exposure models for traffic related NO<sub>2</sub> across geographically diverse areas over separate years *Atmos. Environ.* **46** 460–71
- Mahato S, Pal S and Ghosh K G 2020 Effect of lockdown amid COVID-19 pandemic on air quality of the megacity Delhi, India *Sci. Total Environ.* **730** 139086
- Manoli G et al 2019 Magnitude of urban heat islands largely explained by climate and population *Nature* **573** 55–60
- Meng X et al 2015 A land use regression model for estimating the NO<sub>2</sub> concentration in Shanghai, China *Environ. Res.* **137** 308–15
- Minoura H and Ito A 2010 Observation of the primary NO<sub>2</sub> and NO oxidation near the trunk road in Tokyo *Atmos. Environ.* **44** 23–9
- Mohegh A, Goldberg D, Achakulwisut P and Anenberg S C 2020 Sensitivity of estimated NO<sub>2</sub>-attributable pediatric asthma incidence to grid resolution and urbanicity *Environ. Res. Lett.* **16** 014019
- National Weather Service 2020 Addition Köppen-Geiger climate subdivisions (available at: [https://weather.gov/jetstream/climate\\_max](https://weather.gov/jetstream/climate_max))
- Open Weather 2020 We deliver 2 billion forecasts per day (available at: <https://openweathermap.org/>)
- OpenStreetMap 2020 A map of the world under an open license (available at: <https://openstreetmap.org>)
- Palmgren F, Berkowicz R, Ketzel M and Winther M 2007 Elevated NO<sub>2</sub> pollution in Copenhagen due to direct emission of NO<sub>2</sub> from road traffic *2nd ACCENT Symp. (Urbino, Italy, 23–27 July)*
- Shon Z H, Kim K H and Song S K 2011 Long-term trend in NO<sub>2</sub> and NO<sub>x</sub> levels and their emission ratio in relation to road traffic activities in East Asia *Atmos. Environ.* **45** 3120–31
- Shrestha A M et al 2020 Lockdown caused by COVID-19 pandemic reduces air pollution in cities worldwide *EarthArXiv* (<https://doi.org/10.31223/osf.io/edt4j>)
- Singer G, Zivin J G, Neidell M and Sanders N 2020 Air pollution increases influenza hospitalizations *medRxiv* (<https://doi.org/10.1101/2020.04.07.20057216>)
- Singh S N and Mohapatra A 2019 Repeated wavelet transform based ARIMA model for very short-term wind speed forecasting *Renew. Energy* **136** 758–68
- State Space Methods 2020 Seasonal AutoRegressive integrated moving average with eXogenous regressors model (available at: <https://statsmodels.org/dev/generated/statsmodels.tsa.statespace.sarimax.SARIMAX.html>)
- Tang J et al 2019 Assessing the impact of vehicle speed limits and fleet composition on air quality near a school *Int. J. Environ. Res. Public Health* **16** 149
- UN News 2020 UN launches COVID-19 plan that could ‘defeat the virus and build a better world’ (available at: <https://news.un.org/en/story/2020/03/1060702>)
- Valipour M 2015 Long-term runoff study using SARIMA and ARIMA models in the United States *Meteorol. Appl.* **22** 592–8
- Velders G J and Diederens H S 2009 Likelihood of meeting the EU limit values for NO<sub>2</sub> and PM<sub>10</sub> concentrations in the Netherlands *Atmos. Environ.* **43** 3060–9
- Venter Z S, Aunan K, Chowdhury S, Lelieveld J 2020 COVID-19 lockdowns cause global air pollution declines *PNAS* **117** 18984–90
- Wang Y et al 2020 Spatial decomposition analysis of NO<sub>2</sub> and PM<sub>2.5</sub> air pollution in the United States *Atmos. Environ.* **241** 117470
- Zhao L, Lee X, Smith R B and Oleson K 2014 Strong contributions of local background climate to urban heat islands *Nature* **511** 216–19
- Zhu Y, Jing X, Fengming H and Liqing C 2020 Association between short-term exposure to air pollution and COVID-19 infection: evidence from China *Sci. Total Environ.* **727** 138704